Desalination and Water Treatment
www.deswater.com

doi: 10.5004/dwt.2017.21360

90 (2017) 99–109
September

Fouling characterization of TiO_2 nanoparticle embedded polypropylene membrane in oil refinery wastewater treatment using membrane bioreactor (MBR)

Milad Fonouni[a,b], Habib Etemadi[a,b], Reza Yegani[a,b,*], Saber Zarin[a,b]

[a]*Faculty of Chemical Engineering, Sahand University of Technology, Tabriz, Iran, emails: ryegani@sut.ac.ir (R. Yegani), miladfonouni@gmail.com (M. Fonouni), etemadi.habib@yahoo.com (H. Etemadi), zarrinsaber@yahoo.com (S. Zarin)*
[b]*Membrane Technology Research Center, Sahand University of Technology, Tabriz, Iran*

Received 12 January 2017; Accepted 22 August 2017

ABSTRACT

TiO_2 nanoparticles embedded polypropylene (PP) membranes were fabricated via thermally induced phase separation method. Different amounts of TiO_2 nanoparticles (0–1 wt%) were added to the PP membranes and the optimum composition (0.75 wt% of TiO_2 in the casting solution) was selected according to the several structural and operational analyses. The performance and antifouling behavior of the optimized nanocomposite membrane were examined using submerged membrane bioreactor (MBR) system in treatment of primary effluent obtained from the wastewater treatment unit of Tabriz Oil Refinery Co. (Iran). The obtained results confirmed that the addition of TiO_2 nanoparticles improves the thermal, mechanical and operational properties of PP membrane. For instance, critical flux increased from 34.5 to 64 L/m^2 h for neat and nanocomposite membranes, respectively. Intrinsic, cake layer and irreversible fouling resistances decreased from 73.50, 511.11 and 756.01 to 25.01, 224.58 and 315.00 for neat and nanocomposite membrane, respectively. Using Hermia's fouling model, it was shown that the governing fouling mechanism is cake formation for both membranes; however, the portion of irreversible fouling considerably decreased when nanocomposite membrane was utilized. The conspicuous reduction in the fouling of nanocomposite membrane introduces the great potential of this membrane to be used in MBR for wastewater treatment.

Keywords: Membrane bioreactor; TiO_2 nanoparticle; Polypropylene membrane; Nanocomposite membrane; Membrane fouling; TIPS method

1. Introduction

Recently, due to continual population growth, agricultural and industrial development and climate change effects, water resources' scarcity has become a critical issue in many parts of the world. Water reclamation and reuse in urban areas and industries is becoming an important element of water supply portfolio as wastewater is a reliable and sustainable water source [1]. Membrane bioreactor (MBR) which integrates conventional activated sludge process with membrane separation has been widely used for both industrial and urban wastewater treatments [2–7]. The important advantage of the MBR technology is considered to be its compactness, as the clarifier, where the separation of the sludge from the treated effluent occurs conventionally by gravity, is substituted by a membrane filtration which can be directly implemented in the aerated biological reactor. Beside, due to low sludge production and high permeate quality that can be suitable for reuse, MBRs have gained much attention [8–13]. Nevertheless, membrane fouling is an inevitable problem and remains one of the major obstacles to treated water readily available to reclamation and reuse by MBRs [14–16]. The considerations and findings providing insight to fouling behavior in such complicate environments are investigated in the broad circumstances of observations and tools commonly used to explore them. Among numerous aspects, we have mainly focused on the impact of membrane material with more concentration on the fouling mechanism and its influence on the critical and sustainable flux in such a

* Corresponding author.

mixed species medium because it has been reported that critical flux significantly affects on membrane fouling and MBR operation [17].

Since hydrophobic adsorption of sludge constituents such as sludge flocs, colloids and soluble microbial products (SMP) and extracellular polymeric substances (EPS) on membrane surfaces plays a key role in membrane fouling [18–20], it seems possible to mitigate membrane fouling by increasing the hydrophilicity of the membrane. As a result, much attention has been paid to reducing membrane fouling by modifying hydrophobic materials to relative hydrophilic properties [21–24].

Polyolefin-based polymeric membranes such as polypropylene (PP) exhibit exceptional abilities regarding resistance in various acidic and alkaline solutions; suitability for operation and washing procedures in MBR technology, cost-effectiveness, high stiffness and good tensile strength [25,26]. However, they suffer from poor functionality, which restricts their application in many industries and processes. Their intrinsic hydrophobic nature causes them to be easily fouled in MBR. Therefore, it would be natural to modify membrane to obtain better performance.

Ultraviolet irradiation [27], blending with hydrophilic materials [18], graft polymerization [28] and plasma grafting [29] are reported as the most common membrane modification methods. Among these methods, blending with hydrophilic materials, especially hydrophilic nanoparticles can significantly alleviate membrane fouling [30]. Blending modification with inorganic nanoparticles as well as accomplishing membrane preparation and hydrophilic modification process in one step has shown a good merit to be chosen as an efficient membrane modification method. Moreover, using blending, the modified membrane can obtain the basic properties of organic and inorganic materials and offer specific advantages for the preparation of membranes with excellent separation performance, good thermal and chemical resistance and adaptability to harsh environments [30]. Results have shown that membrane modifications by hydrophilic titanium dioxide (TiO_2) [31], alumina (Al_2O_3) [32] and graphene oxide (GO) [17] can significantly improve hydrophilic property and reduce membrane fouling in MBR.

Homayoonfal et al. [32] studied polysulfone/alumina nanocomposite membranes performance in MBR with the aim of reducing biofouling. Their results indicated that alumina nanoparticles can increase water flux by enhancing membrane hydrophilicity while maintaining the separation efficiency through decreasing the membrane porosity. Zhao et al. [17] compared the performance of polyvinylidene fluoride (PVDF)/GO composite microfiltration membrane with commercial PVDF membrane in MBR. Their results revealed that composite microfiltration membrane showed lower membrane resistance, particularly lower pore plugging resistance than commercial PVDF membrane.

Among different inorganic nanoparticles, TiO_2 has received most of the attention because of its unique specifications such as stability under harsh conditions, commercial availability and easiness of preparation. PP membrane blending modification with TiO_2 nanoparticles and its application in MBRs, however, have not been extensively studied or reported. Bae and Tak [33] investigated the effect of TiO_2 nanoparticles on the fouling mitigation of polysulfone, polyacrylonitrile and PVDF ultrafiltration membranes. They concluded that nanocomposite polymer membranes showed lower flux decline compared with that of neat polymeric membrane, membrane fouling was mitigated by TiO_2 immobilization.

Antifouling properties and fouling mechanisms of fabricated membrane have been usually investigated using synthetic influents or model wastewater stream and the lack of experimental data using real wastewater streams is still inevitable.

Herein, we report the fabrication of PP/TiO_2 nanocomposite membrane via thermally induced phase separation (TIPS) method. The fouling mechanism as well as antifouling performance of fabricated membrane was investigated using oil refinery wastewater influents obtained from Tabriz Oil Refinery Co. in locally manufactured MBR unit with a purification capacity of 100 L/d. The filtration behavior was further analyzed in MBR and the impact of membrane type on the critical flux was investigated and the obtained results were also modeled with Hermia and resistance in series (RIS) methods. In addition, a set of analyses including scanning electron microscopy (SEM), thermogravimetric analysis (TGA), static contact angle (CA) measurement, mechanical strength, pure water flux (PWF), porosity and pore-size distribution measurement were carried out to fully characterize the membrane.

2. Materials and methods

2.1. Experimental setup

A lab-scale in-house manufactured aerobic MBR with a working volume of 20 L was used (Fig. 1). As shown in Fig. 1, it consists of an aerated reactor with submerged flat-sheet microfiltration membrane modules and feed tank.

A dead-end polyimide flat-sheet membrane module providing 14 cm^2 of filtration area was submerged in the aerobic bioreactor (Fig. 2).

An air diffuser was installed beneath the membrane module to provide dissolved oxygen as well as efficient agitation of activated sludge in the MBR. The air bubbles generated during aeration with the flow rate of 0.5 L/min, on the other hand, induced a cross-flow scouring the membrane surface which removed attached sludge flocs and subsequently suppressed membrane fouling. To eliminate the influence

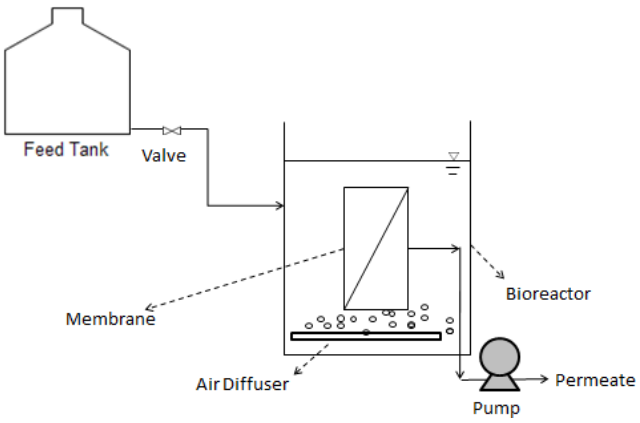

Fig. 1. A schematic view of the membrane bioreactor used to analyze the membrane.

of different physiological states of the activated sludge suspension on the filtration performance, all membrane modules were installed into the MBR at the same time. The MBR was fed with primary effluent obtained from the wastewater treatment unit of Tabriz Oil Refinery Company (TZ.O.R.C), Tabriz, Iran, and operated in the constant conditions. Details of the operational conditions and composition of the real wastewater are listed in Table 1.

The critical flux was determined using transmembrane pressure (TMP) step method reported by Gesan-Guiziou et al. [34]. The step by step technique consisted of methodical increase of TMP (30 min at each TMP step before the critical flux was reached 15 min afterwards), the first unstable permeation flux was determined when J decreased over the course of time, resulting in non-linearity in the J vs. TMP [34].

In this study, all of the experiments were carried out after the MBR was acclimated for three solid retention time (SRT) to ensure the stability of sludge characteristics. The SRT of the MBR was maintained at almost 20 d and the mixed liquid of suspended solids (MLSS) stabilized at around 7,000–7,500 mg/L. After three SRT, the critical flux was measured.

2.2. Materials

The utilized materials either for dope solution or for nanoparticles additives are very cheap among conventionally utilized initial materials for membrane fabrication. Isotactic PP with commercial grade (EPD60R, MFI = 0.35 g/10 min) was purchased from Arak Petrochemical Co., Iran. TiO_2 nanoparticles (particle size of ca. 21 nm) were purchased from Sigma-Aldrich (Germany). Mineral oil as diluent, acetone as extracting agent and Irganox 1010 as heat stabilizer were purchased from Acros Organics (Belgium), Merck (Germany) and Ciba Co. (Switzerland), respectively. All materials were used as-received unless otherwise described.

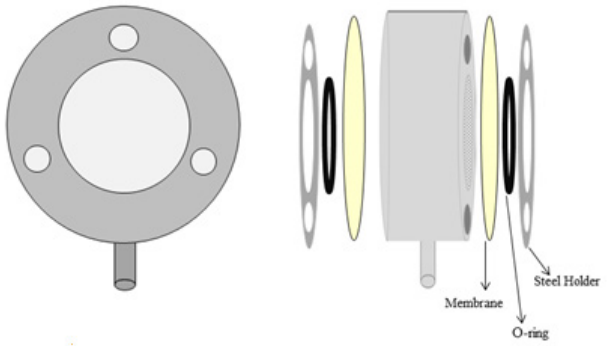

Fig. 2. Schematic of flat-sheet membrane module.

Table 1
Specification of wastewater stream and operating conditions of MBR

Parameters	Values
Hydraulic retention time (HRT, h)	24
Solid retention time (SRT, d)	20
Mixed liquor suspended solids (MLSS, mg/L)	7,000
pH	6.8–7.6
Feed concentration (mg COD/L)	178
Temperature	Room temperature
Air flow rate (L/min)	0.5
Working volume (L)	20

2.3. Membrane preparation

TIPS method was applied to prepare neat and PP/TiO_2 nanocomposite membranes. Precise amounts of TiO_2 nanoparticles (0.25, 0.50, 0.75 and 1 wt%) with Irganox (1 wt% of solid phase) were dispersed into 60 g of mineral oil using bath sonication (Woson, China) for 60 min. Then, PP powder was added to the diluent-nanoparticle suspension and melt blended at 170°C for 90 min in a sealed glass vessel kept in a silicon oil bath. The solution was then allowed to degas for 30 min and cast on a preheated glass sheet using a doctor blade. The plate was immediately quenched in the water bath (30°C ± 3°C) to induce phase separation. The membrane was then immersed in acetone for 24 h to extract its diluent. The results of differential scanning calorimetry analysis revealed that the acetone in the membranes was removed during drying at room temperature (data not shown, fabrication procedure is already fixed in this laboratory [35]).

2.4. Membrane characterization

2.4.1. Static contact angle measurement

The hydrophilic property of PP/TiO_2 nanocomposite membranes was evaluated by measuring the CA between membrane surface and water droplet using a CA goniometer (PGX, Thwing-Albert Instrument Co., USA). To minimize experimental error, the CAs were measured at five random locations for each sample and the average number was reported.

2.4.2. Porosity

Membrane porosity was determined according to its dry–wet weight. As reported in literature, PP membranes were immersed in *i*-butanol for 24 h and then immediately weighed after removing *i*-butanol from the surface. The porosity was calculated using the following equation [36]:

$$\varepsilon = \frac{(W_2 - W_1)\rho_1}{\rho_1 W_2 + (\rho_2 - \rho_1)W_1} \times 100 \quad (1)$$

where W_1 is the initial membrane weight, W_2 is the membrane weight after 24 h immersion in *i*-butanol, ρ_1 and ρ_2 are the density of PP (0.91 g/cm^3) and *i*-butanol (0.8 g/cm^3), respectively.

2.4.3. Tensile strength

The tensile strength of the fabricated PP/TiO_2 nanocomposite membranes was determined by using a tensile testing machine (STM-5, Santam, Iran) at an extension rate of 10 mm/min. The samples were cut into 8 cm × 1.5 cm in

length and width, respectively. The thickness of each sample was measured by a micrometer. Three trials were carried out for each sample and the mean values were reported.

2.4.4. Thermogravimetric analysis

Thermogravimetric analyzer (TGA Q-50, TA Instruments, UK) was used to study the effect of TiO_2 on the thermal stability of nanocomposite membrane and homogenous distribution of nanoparticles in membrane. Approximately, 10 mg of the samples were heated at a rate of 20°C/min from ambient to 800°C. The chamber was continuously swept with nitrogen at a rate of 90 mL/min. The corresponding weight changes were noted with the help of an ultrasensitive microbalance. In order to investigate the homogenous distribution of nanoparticles, three different pieces of three different parts of flat-sheet membrane were selected and TGA analysis was carried out.

2.4.5. Pure water flux

PWF of membranes was determined using an in-house fabricated dead-end filtration system with 14 cm^2 of membrane area. Since polymeric membrane can be compacted by the pressure applied during filtration, the flux can be reduced without membrane fouling. Thus, all membranes were previously filtered by pure water until the flux reached steady state before the MBR fouling tests in order to eliminate the compaction effect on the flux decline. PWF was measured at 100 kPa under steady-state flux rate and calculated by the following equation:

$$J_0 = \frac{V}{A.t} \tag{2}$$

where J_0 is the PWF, V the collected volume of water (L), A the membrane area (m^2) and t is the time (h).

2.4.6. Pore-size distribution measurement

Image analysis was performed to count the cell size and cell size distribution of each sample. In order to achieve reliable data, two SEM images were taken of each sample and ImageJ software was used to count cell size distribution. From two SEM images taken of each sample, an equal number of cells measured and average data was reported.

2.5. Analytical methods

Fouling can be quantified by the resistance appearing during filtration and cleaning. The degree of membrane fouling was calculated quantitatively using RIS model [37]:

$$J = \frac{\Delta P}{\eta R_t} \tag{3}$$

where J is the permeation flux (m^3/m^2 s), ΔP is the TMP (Pa), η is the viscosity of permeate (Pa s) and R_t is the total filtration resistance (m^{-1}). Total resistances (R_t) were reclassified into three parts:

$$R_t = R_m + R_C + R_f \tag{4}$$

where R_m is the intrinsic membrane resistance, R_c is the resistance due to cake layer formed on membrane surface and R_f is the fouling resistance caused by pore plugging and irreversible adsorption of foulants on membrane pore wall or surface. Those resistances can be calculated from experimental data using the following equations:

$$R_m = \frac{\Delta P_T}{\eta J_w} \tag{5}$$

$$R_f = \frac{\Delta P_T}{\eta J_{aw}} - R_m \tag{6}$$

$$R_c = \frac{\Delta P_T}{\eta J_{as}} - R_m - R_f \tag{7}$$

where J_{as} is the flux at steady state in MBR, J_w is the initial water flux and J_{aw} is the final water flux after removing cake layer. Cake layer was removed by flushing with tap water.

The mode of permeate flux decline during filtration process can be identified by the following equation [38]:

$$\frac{d^2t}{dV^2} = k\left(\frac{dt}{dV}\right)^m \tag{8}$$

where V is the cumulative volume of filtrate, t is the time of filtration operation and k is a constant value. The permeate flux is presented as follows [39]:

$$J = \frac{1}{A}\frac{dV}{dt} \tag{9}$$

This can be written as:

$$\frac{dt}{dV} = \frac{1}{A.J} \tag{10}$$

Taking derivative of Eq. (10) with respect to t and substituting in Eq. (8) results to the governing equation of flux decline with time as follows:

$$\frac{dJ}{dt} = -kJ^{3-m} \tag{11}$$

where k is a constant value and m is a general index, which depends on the fouling mechanism. The values of n varied from 0 to 1, 1.5 and 2 for cake formation, intermediate blocking, pore constriction and complete blocking, respectively.

The proposed mechanisms for all fouling models are explained in detail in literature [40]. The analytical solutions of Eq. (11) for each m value as well as the linear forms of flux expressions are listed in Table 2 [41]. The governing mechanisms of fouling in MBR are also explained by fouling models, which are derived from Hermia's model but in a specific context. In this study, we chose to use Hermia's models to determine, with an optimization approach, the most likely fouling modes in an MBR. It is required to state here that the chemical oxygen demand (COD) analysis was carried out in the central laboratory of Tabriz Oil Refinery Co.

Table 2
Summary of the fouling mechanisms and blocking models during membrane fouling

Type of blocking	Fouling concept	*M*	Flux expression	Linear form
Cake formation	Formation of cake layer on surface	0	$J = \frac{J_0}{(1+J_0kt)^{0.5}}$	$\frac{1}{J^2} = \frac{1}{J_0^2} + kt$
Intermediate blocking	Pore sealing and membrane surface deposition	1	$J = \frac{J_0}{(1+J_0kt)}$	$\frac{1}{J} = \frac{1}{J_0} + kt$
Pore constriction	Pore wall restricted	1.5	$J = \frac{J_0}{(1+J_0^{0.5}kt)^2}$	$\frac{1}{\sqrt{J}} = \frac{1}{\sqrt{J_0}} + kt$
Complete pore blocking	Pore sealing	2	$J = J_0 \exp(-kt)$	$\ln\left(\frac{1}{J}\right) = \ln\left(\frac{1}{J_0}\right) + kt$

3. Results and discussion

3.1. Static contact angle, porosity, pure water flux and pore-size distribution

It has been shown that membrane hydrophilicity, microstructure, material and pore-size distribution were all significantly influencing MBR fouling [42]. Therefore, in this section the abovementioned parameters were investigated and compared for neat and TiO_2 embedded membranes to find the optimum composition for further operational and performance considerations.

CA represents the wettability of surface and depends on the surface hydrophilicity and roughness. The CA results of PP and PP/TiO_2 nanocomposite membranes are given in Fig. 3. The PP/TiO_2-0.75 membrane showed lower CA compared with pristine PP and PP/TiO_2 nanocomposite membranes.

The relatively higher hydrophilicity of PP/TiO_2 nanocomposite membranes compared with pristine PP membrane can be ascribed to the presence of TiO_2 nanoparticles, which contain a great deal of hydroxyl functional groups responsible for the hydrophilicity increase and consequently higher affinity of metal oxide to water [33]. The decrease in CA, however, was not prominent, which is attributed to the impact of surface roughness. Our previous findings revealed that incorporation of hydrophilic TiO_2 nanoparticles is expected to increase the hydrophilicity, decrease the CA and increase the surface roughness of polyolefin-based membrane. However, according to the Wenzel model, the degree of roughness should be such to amplify the wettability of the surface toward its intrinsic tendency, therefore two aforementioned contrary factors controlling the final CA balance the hydrophilic property of TiO_2 particles with membrane surface roughness [43].

The porosity of PP and PP/TiO_2 nanocomposite membranes is given in Fig. 4. Due to the fact that the addition of TiO_2 nanoparticles could accelerate the crystallization rate and act as the crystal nuclei at the low quenching temperature [44], the average pore size and the porosity of nanocomposite membrane could be higher than those of the nascent PP membrane.

The influence of TiO_2 nanoparticle content on permeability was also investigated through PWF experiments.

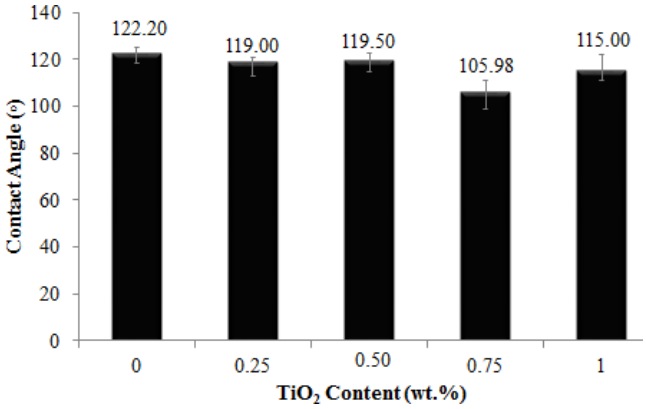

Fig. 3. The effect of nanoparticles concentrations on the contact angle of PP and PP/TiO_2 nanocomposite membranes.

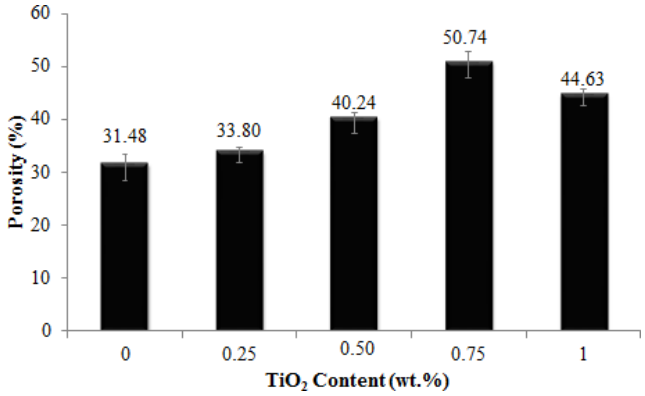

Fig. 4. The effect of nanoparticles concentrations on the porosity of the PP and PP/TiO_2 membranes.

A similar trend with porosity was also obtained for the PWF shown in Fig. 5. PWF results revealed that the permeability of the membranes was enhanced by increasing TiO_2 concentration, with a peak value at 0.75 wt% TiO_2. The PWF of membranes increased from 50.28 L/m² h for pristine PP membrane to a peak value of 147.69 L/m² h for PP/TiO_2-0.75 nanocomposite membrane which was about 2.93 times higher than

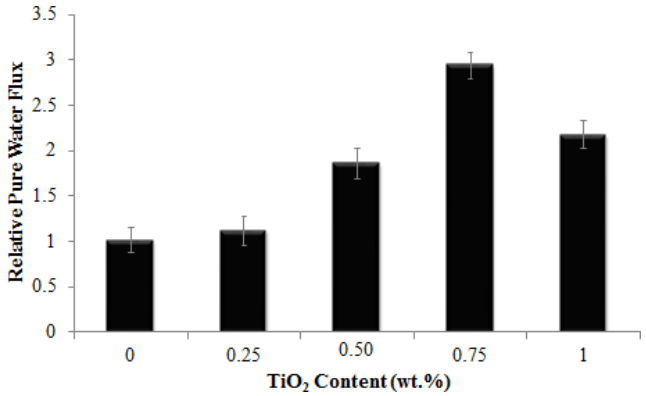

Fig. 5. The effect of nanoparticles concentrations on the pure water flux of PP and PP/TiO_2 membranes.

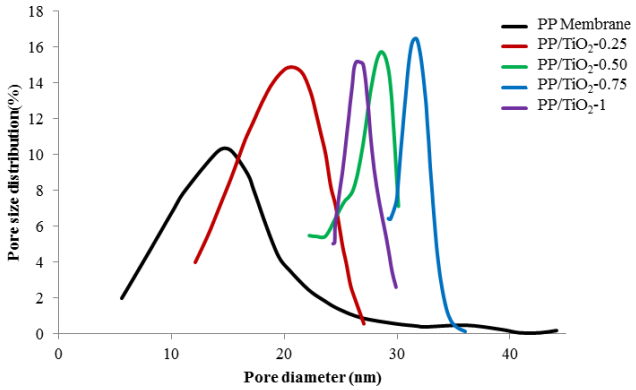

Fig. 6. Pore-size distributions of the membranes with various TiO_2 contents.

that of pristine PP membrane. However, a higher content of TiO_2, that is, 1 wt%, led to a decrease in PWF. According to our previous findings [43], it is mainly attributed to the fact that at high TiO_2 nanoparticle dosage, agglomeration of TiO_2 nanoparticles in PP matrix restrained the formation of spherulites and led to less pores and lower porosity in nanocomposite membrane. In the PP/TiO_2-0.75 nanocomposite membrane, TiO_2 nanoparticles expose the lowest aggregation and the highest adsorbed –OH or hydrophilicity [45]. Low aggregation and high hydrophilicity led to higher PWF. The obtained results suggest that there is an optimum value of TiO_2 fraction for PWF.

Fig. 6 shows the pore-size distribution of 0–1 wt% PP/TiO_2 nanocomposite membranes. The results showed that the addition of different amounts of TiO_2 changes the pore-size distribution of PP/TiO_2 nanocomposite membrane. While the pore-size distribution shifts toward larger pore size by increasing TiO_2 content up to 0.75 wt% TiO_2, the pore-size distribution moves back to smaller pore size for the PP/TiO_2-1 membrane. The obtained results are in good agreement with the PWF results; they clearly explain the decrease in PWF of the membrane with 1 wt% TiO_2 nanoparticles in Fig. 5.

3.2. Mechanical behavior of membranes

Addition of nanoparticles into polymeric membrane changes the mechanical properties of polymeric membrane. Fig. 7 illustrates the effect of nanoparticles incorporation on the membrane mechanical resistance behavior.

According to the obtained results, the mechanical strength of pristine PP membrane increased by following the addition of nanoparticle. Similar to our previous findings [43], this manner can be attributed to the crystallinity change in PP and the reinforcement effect of the inorganic nanoparticles due to the addition of nanoparticle. The mechanical properties of the nanocomposites, however, depend significantly on their internal structure. It may be due to the poor compatibility of hydrophilic TiO_2 nanoparticles with a hydrophobic polymer matrix, in higher extent of inorganic nanoparticles, the polymer nanocomposites are difficult to reach without particle aggregates and/or agglomerates. Besides, there is no chemical bond between nanoparticles and polymer chains. Thus, the applied load was hardly transferred from

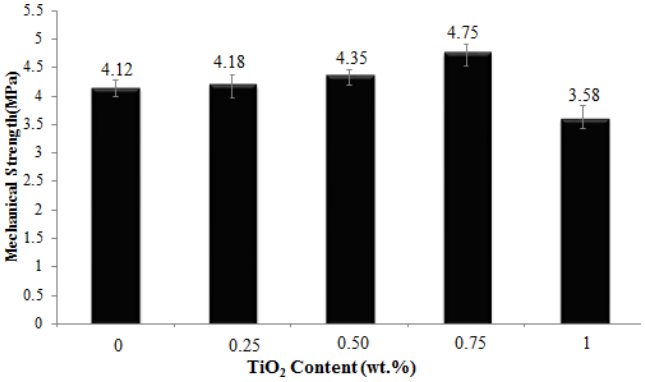

Fig. 7. The effect of nanoparticles concentrations on the mechanical strength of PP and PP/TiO_2 membranes.

polymer to fillers in higher amount of nanoparticles [46]. The non-uniform distribution of nanoparticles throughout the PP matrix and no significant organic–inorganic interaction are major factors that affect tensile strength of nanocomposite membranes.

3.3. Morphological studies of membranes

Among several fabricated nanocomposite TiO_2 embedded PP membrane, PP/TiO_2-0.75 membrane was selected for further structural and operational analyses due to its maximum PWF, higher porosity and hydrophilicity and also desirable mechanical strength.

The surface morphology of pristine PP membrane and the selected membrane, PP/TiO_2-0.75, is shown in Fig. 8.

As predicted, addition of TiO_2 nanoparticles increased the nucleation density and led to the formation of porous as well as more uniform spherulites in PP/TiO_2-0.75 nanocomposite membranes than those in pristine PP membranes. It is mainly due to the fact that TiO_2 nanoparticles acted as the crystal nuclei and a certain amount of TiO_2 dosage could increase the number of spherulites, decrease the size of spherulites and caves between the spherulites and make spherulites more uniform. Fig. 8 also shows that the addition of TiO_2 nanoparticles increased the number and the size of pores in the surface of membranes. This may be due to the heterogeneous nucleation effect of TiO_2 nanoparticles.

The cross-section SEM images of the membrane samples in two magnifications are shown in Fig. 9. SEM images show that, compared with neat PP membrane, by addition of TiO_2 nanoparticles, porosity and pore size of PP/TiO_2-0.75 nanocomposite membrane increased.

PP membrane usually shows the spherulitic morphology. The spherulitic morphology was the typical structure of solid–liquid phase separation via nucleation and crystal growth [35]. Due to the fact that the addition of TiO_2 nanoparticles could accelerate the crystallization rate and acted as the crystal nuclei at low quenching temperature [44]. Therefore, the average pore size and porosity of nanocomposite membrane could be higher than those of the nascent PP membrane.

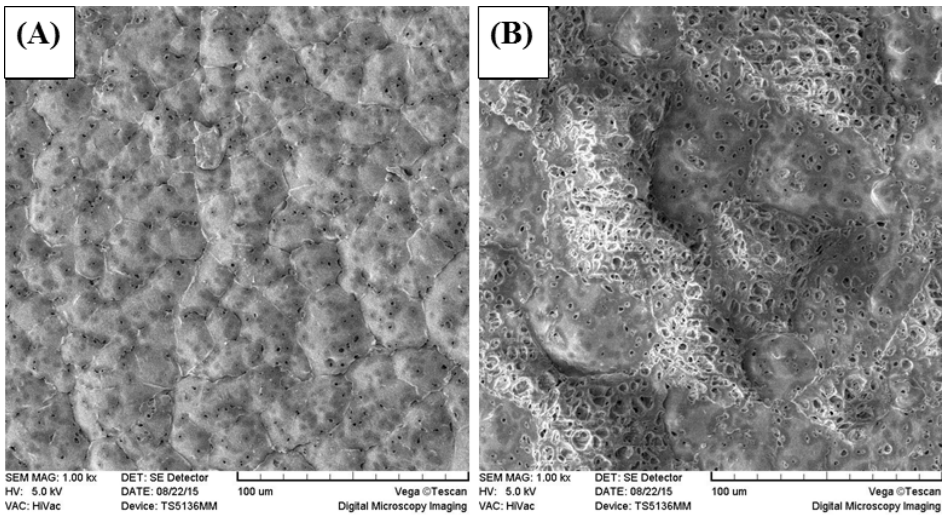

Fig. 8. SEM images of the surfaces of the (A) pristine PP membrane and (B) PP/TiO_2-0.75 nanocomposite membrane.

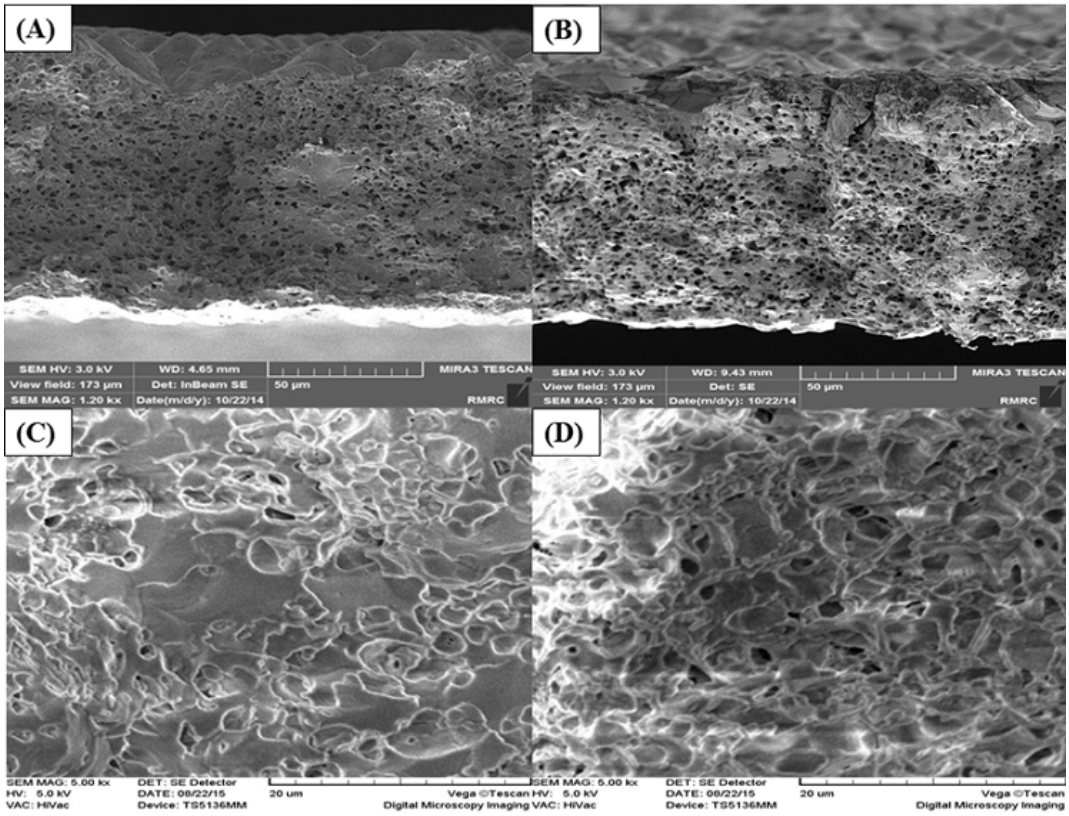

Fig. 9. FESEM images of the cross-sections of the (A) pristine PP membrane, (B) PP/TiO_2-0.75 nanocomposite membrane, (C) pristine PP membrane with high resolution and (D) PP/TiO_2-0.75 nanocomposite membrane with high resolution.

3.4. Thermogravimetric analysis

Due to the lower amount of TiO_2 nanoparticle in the bulk of fabricated membrane, XRD analysis could not confirm the existence of nanoparticles. Therefore, TGA was carried out to evaluate both thermal stability and homogenous distribution of nanoparticles in pristine PP and PP/TiO_2-0.75 membranes. TGA results are shown in Fig. 10. From the TGA curves, it can be found that the nanofiller significantly improves the thermal stability of PP.

As can be seen from the figure, the pristine membrane starts to decompose at 211°C and ends at 384°C. The PP/TiO_2-0.75 nanocomposite membrane, however, begins to decompose at a relatively higher temperature of 248°C and ends at 440°C. The increase in the onset temperature of nanocomposite membrane can be attributed to the presence of TiO_2 nanoparticles. TiO_2 nanoparticles are capable of restricting the movement of a polymer chain, making the scission of polymer chains harder at lower temperatures. As a consequence, the degradation temperature of the PP/TiO_2-0.75 membrane shifts to higher temperatures. In addition, the difference between weight losses of three specimens for each sample was <1%, which confirms the good settlement of nanoparticle in PP membrane. It can be concluded that the distribution of TiO_2 nanoparticles in the bulk of the membrane has been successfully achieved.

3.5. Critical fluxes of PP and PP/TiO_2 nanocomposite membranes

The critical fluxes of both membranes were measured through the step by step technique. As shown in Fig. 11, the critical flux of PP/TiO_2 nanocomposite, 60–68 L/m^2 h, was significantly higher than that of neat PP membrane, 34–35 L/m^2 h.

As reported in the literature, critical flux strongly depends on the membrane characteristics such as pore-size distribution, membrane materials, surface hydrophilicity and feed properties as well as operation conditions [17]. In this work, the PP/TiO_2 nanocomposite membrane showed larger pore size, relative hydrophilicity and improved PWF, which consequently resulted in higher critical flux.

3.6. MBR performance

Since usual wisdom generally ascribes lower fouling to hydrophilic membranes with high porosity and narrow pore-size distribution, lower fouling is expected to be observed for

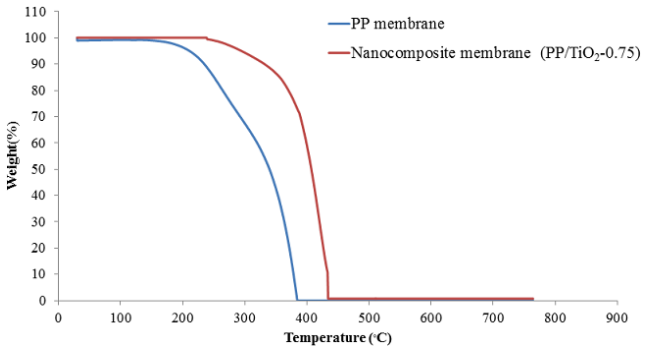

Fig. 10. TGA thermographs of pristine PP membrane and PP/TiO_2-0.75 nanocomposite membrane.

TiO_2 embedded nanocomposite membrane. The influence of pore size on the fouling, however, was found to differ in various studies [47]. Therefore, fouling analyses were carried out to monitor the mechanism of fouling for neat and modified membranes.

The various filtration resistances were calculated for PP and PP/TiO_2-0.75 membranes in MBR and the results are shown in Table 3.

Fouling in MBR could be characterized by an outer cake layer on the membrane surface and an inner gel layer in the membrane. Cake layer from MLSS, which contributes to reversible fouling and the cake resistance (R_c), can be easily removed by a physical cleaning. The inner gel layer formed by strongly attached SMP or EPS blocks and clogs pores contributes to the irreversible fouling resistance (R_f) that can only be removed by chemical cleaning.

In comparison with pristine PP membrane, the PP/TiO_2-0.75 nanocomposite membrane showed lower membrane resistance (65.97% of the pristine PP membrane). A detailed analysis revealed that the cake layer was the major fouling

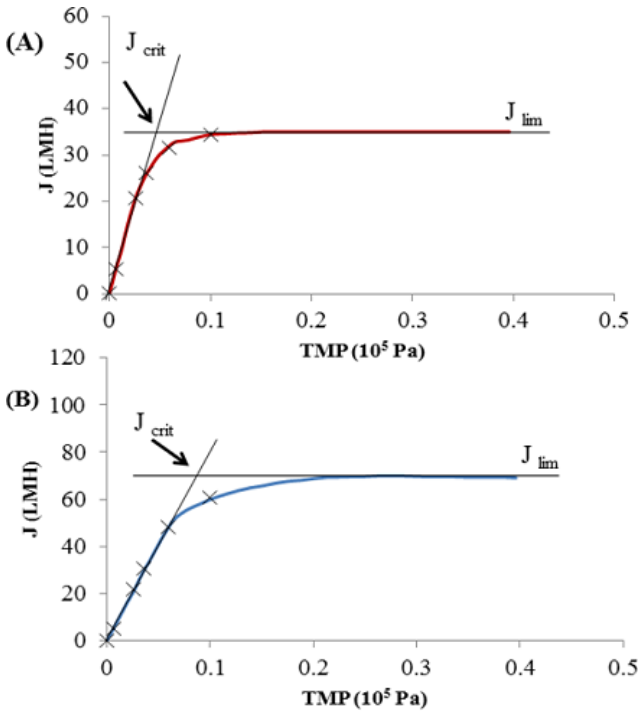

Fig. 11. Determination of the critical flux for (A) pristine PP membrane and (B) PP/TiO_2-0.75 nanocomposite membrane using TMP-step method.

Table 3
Filtration resistances of pristine and PP/TiO_2-0.75 nanocomposite membranes

Membranes	R_m (×10^{11} m^{-1})	R_c (×10^{11} m^{-1})	R_f (×10^{11} m^{-1})	R_t (×10^{11} m^{-1})
PP	73.50	511.11	171.40	756.01
PP/TiO_2-0.75	25.01	224.58	65.41	315.00

contributor for both membranes (71.29% for the nanocomposite membrane and 67.60% for the pristine PP). As mentioned above, since PP and PP/TiO_2-0.75 nanocomposite membranes were tested at the same condition, the surface properties of membrane were the only key factor to determine the amount of cake layer resistance. Since the incorporation of nanoparticles increased the hydrophilicity of the polymeric membrane surface, the decrease in cake layer resistance strongly suggested that the adsorbed foulants on the nanocomposite membrane could be more readily dislodged by shear force than those attached on a pristine PP membrane. The R_f of nanocomposite membrane caused by pore clogging and irreversible fouling was significantly lower than that of PP membrane (61.83% that of the pristine PP membrane). Due to the hydrophilic modification of the membrane by the incorporation of TiO_2, the hydrophobic interaction between organic foulants and the membrane surface diminished.

In order to find the best model to describe membrane fouling in MBR, the values of the k factor for different values of m of pristine PP and PP/TiO_2-0.75 membranes were determined by using the least square method. The experimental data were substituted in the linearized equations, shown in Table 4, and k value was obtained as the slope of the line. After that, with k values on other hand, the flux equations in Table 3 were plotted for each filtration test and compared with experimental data.

The best fouling model was selected based on the equation best fitted with the highest value of R^2 in linear regression method. Comparison between experimental data and fouling models for pristine PP and PP/TiO_2-0.75 membranes were shown in Figs. 12(A) and (B), respectively.

The resultant values of k and R^2 are presented in Table 4. In accordance with the results, the experimental data for both membranes were well fitted with cake formation model, since the R^2 values of this model for pristine PP and PP/TiO_2-0.75 membranes were 0.8776 and 0.9528, respectively.

The amount of COD removal for activated sludge and membranes was also investigated and the obtained results were shown in Table 5. It can be observed that COD removal efficiencies of the pristine PP membrane and PP/TiO_2-0.75 nanocomposite membrane were 48.87% and 65.16%, respectively. This efficient reduction in COD can be ascribed to the presence of TiO_2 nanoparticle with bigger pore size and narrow pore-size distribution.

Narrow pore-size distributions decrease the inhomogeneous flow distribution between pores that result in preferential deposition and blockage of large pores [48,49]. Similarly, high porosity corresponding with local flux at the pore entrance will be reduced.

In other words, increasing the pore size may decrease the particle settlement onto the membrane at the expense of internal adsorption. Increasing the pore size also shifts the membrane configuration from ultrafiltration (UF) toward microfiltration (MF) membrane and as reported in the literature, MF membrane seems to rely on the initial fouling in MBR system and the ensuing creation of a dynamic membrane to produce better quality of product, while UF-based membrane in MBR system feature good rejection from the early stage of filtration. However, it was shown that no clear advantage of using tight membranes over more open pores within a range of given flux.

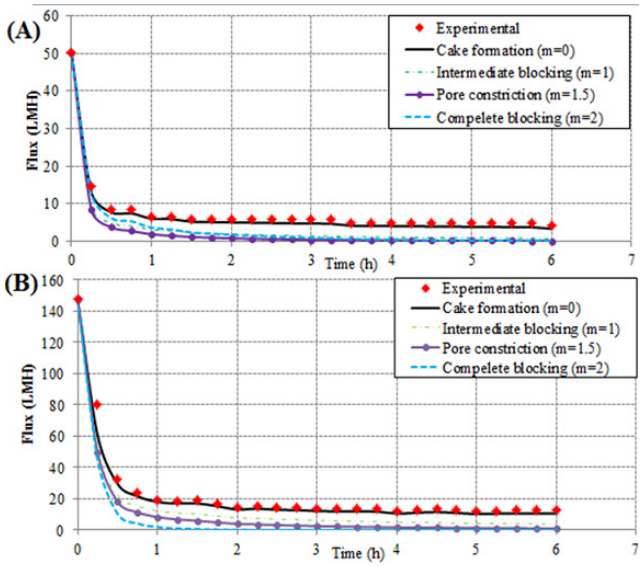

Fig. 12. Experimental filtration data and classic fouling models for membranes in MBR. (A) Pristine PP membrane and (B) PP/TiO_2-0.75 nanocomposite membrane.

Table 5
Comparison of COD values for raw influent, treated influent by CAS, treated influent by MBR using neat PP membrane and treated infleunt by MBR using modified nanocomposite membrane

Sample	COD (mg/L)
Wastewater	178
Wastewater treated with conventional activated sludge	131
Wastewater treated in MBR with PP membrane	91
Wastewater treated in MBR with PP/TiO_2-0.75 nanocomposite membrane	62

Table 4
Values of k in Hermia's fouling models and correlation coefficient of R^2 for membranes

Membrane	$m = 0$		$m = 1$		$m = 1.5$		$m = 2$	
	k	R^2	k	R^2	k	R^2	k	R^2
PP	0.0011	0.8776	0.1117	0.8776	0.5514	0.7403	3.577	0.5885
PP/TiO_2-0.75	0.0001	0.9528	0.0296	0.9265	0.2390	0.8930	2.301	0.7961

4. Conclusions

Fouling is an inevitable problem in membrane processes and still remains one of the major obstacles to wide-spread application of MBR in urban and industrial wastewater treatment. This work explains how to fabricate less fouling membrane using PP as polymer and TiO_2 nanoparticles as additive. The performance of fabricated membrane was examined in the treatment of primary effluent obtained from Tabriz Oil Refinery Co. in a submerged MBR. The obtained results revealed that addition of very little amount of TiO_2 nanoparticles, <1.00 wt%, improves the antifouling property of membrane by decreasing the portion of irreversible fouling and increasing the portion of reversible fouling. It therefore helps the operator to easily wash away the foulants by aeration or chemical cleaning. The obtained results showed that the membrane hydrophilicity, membrane pore size and pore-size distribution are the main influential parameters to affect the membrane performance in MBR.

Acknowledgments

This work was financially supported by Tabriz Oil Refinery Co. They also kindly provided the required samples and carried out the COD tests. The authors specially thank Mr. Gol Sanamlou, Mr. Mohsen Zadeh, Mr. Rezayi and Dr. Zad Ghafari head of R&D center researcher at R&D center, head of wastewater unit and head of technical office of Tabriz Oil Refinery Co. who provided insight and expertise that greatly assisted the research, although they may not agree with all of the interpretations/conclusions of this paper.

References

[1] M.M. Pendergast, E.M. Hoek, A review of water treatment membrane nanotechnologies, Energy Environ. Sci., 4 (2011) 1946–1971.
[2] M.D. Williams, M. Pirbazari, Membrane bioreactor process for removing biodegradable organic matter from water, Water Res., 41 (2007) 3880–3893.
[3] K. Akamatsu, W. Lu, T. Sugawara, S.-i. Nakao, Development of a novel fouling suppression system in membrane bioreactors using an intermittent electric field, Water Res., 44 (2010) 825–830.
[4] S. Gabarrón, G. Ferrero, M. Dalmau, J. Comas, I. Rodriguez-Roda, Assessment of energy-saving strategies and operational costs in full-scale membrane bioreactors, J. Environ. Manage., 134 (2014) 8–14.
[5] G. Di Bella, M. Torregrossa, Foaming in membrane bioreactors: identification of the causes, J. Environ. Manage., 128 (2013) 453–461.
[6] N. Lesage, M. Sperandio, C. Cabassud, Study of a hybrid process: adsorption on activated carbon/membrane bioreactor for the treatment of an industrial wastewater, Chem. Eng. Process., 47 (2008) 303–307.
[7] D. Kwon, H. Chang, H. Seo, J. Kim, Fouling behavior and system performance in membrane bioreactor introduced by granular media as a mechanical cleaning effect on membranes, Desal. Wat. Treat., 57 (2016) 9018–9026.
[8] A. Pollice, C. Giordano, G. Laera, D. Saturno, G. Mininni, Physical characteristics of the sludge in a complete retention membrane bioreactor, Water Res., 41 (2007) 1832–1840.
[9] P. Le-Clech, B. Jefferson, S. Judd, A comparison of submerged and sidestream tubular membrane bioreactor configurations, Desalination, 173 (2005) 113–122.
[10] S. Rosenberger, C. Laabs, B. Lesjean, R. Gnirss, G. Amy, M. Jekel, J.-C. Schrotter, Impact of colloidal and soluble organic material on membrane performance in membrane bioreactors for municipal wastewater treatment, Water Res., 40 (2006) 710–720.
[11] J. Gil, P. Krzeminski, J. Van Lier, J. Van Der Graaf, T. Wijffels, D. Prats, Analysis of the filterability in industrial MBRs. Influence of activated sludge parameters and constituents on filterability, J. Membr. Sci., 385 (2011) 96–109.
[12] P. Karaolia, I. Michael-Kordatou, E. Hapeshi, J. Alexander, T. Schwartz, D. Fatta-Kassinos, Investigation of the potential of a Membrane BioReactor followed by solar Fenton oxidation to remove antibiotic-related microcontaminants, Chem. Eng. J., 310 (2017) 491–502.
[13] R. Aryal, M. Johir, S. Vigneswaran, J. Kandasamy, R. Sleigh, Performance of a stainless steel membrane in membrane bioreactor process, Desal. Wat. Treat., 41 (2012) 258–264.
[14] J. Huang, Z. Wang, J. Zhang, X. Zhang, J. Ma, Z. Wu, A novel composite conductive microfiltration membrane and its antifouling performance with an external electric field in membrane bioreactors, Sci. Rep., 5 (2015) 1–8.
[15] J. Martín-Pascual, P. Reboleiro-Rivas, M.M. Muñio, J. González-López, J.M. Poyatos, Membrane fouling of a hybrid moving bed membrane bioreactor plant to treat real urban wastewater, Chem. Eng. Process., 104 (2016) 112–119.
[16] J. Guo, W. Guan, S. Xia, Membrane fouling of hybrid submerged membrane bioreactor (hMBR) in treating municipal wastewater, Desal. Wat. Treat., 52 (2014) 6858–6867.
[17] C. Zhao, X. Xu, J. Chen, G. Wang, F. Yang, Highly effective antifouling performance of PVDF/graphene oxide composite membrane in membrane bioreactor (MBR) system, Desalination, 340 (2014) 59–66.
[18] T.-H. Bae, T.-M. Tak, Preparation of TiO_2 self-assembled polymeric nanocomposite membranes and examination of their fouling mitigation effects in a membrane bioreactor system, J. Membr. Sci., 266 (2005) 1–5.
[19] T. Jiang, H. Zhang, D. Gao, F. Dong, J. Gao, F. Yang, Fouling characteristics of a novel rotating tubular membrane bioreactor, Chem. Eng. Process., 62 (2012) 39–46.
[20] M. Aslan, Y. Saatçi, Ö. Hanay, H. Hasar, Membrane fouling control in anaerobic submerged membrane bioreactor, Desal. Wat. Treat., 52 (2014) 7520–7530.
[21] J.K. Shim, H.S. Na, Y.M. Lee, H. Huh, Y.C. Nho, Surface modification of polypropylene membranes by γ-ray induced graft copolymerization and their solute permeation characteristics, J. Membr. Sci., 190 (2001) 215–226.
[22] H. Yamagishi, J.V. Crivello, G. Belfort, Development of a novel photochemical technique for modifying poly (arylsulfone) ultrafiltration membranes, J. Membr. Sci., 105 (1995) 237–247.
[23] I. Gancarz, G. Poźniak, M. Bryjak, Modification of polysulfone membranes 1. CO_2 plasma treatment, Eur. Polym. J., 35 (1999) 1419–1428.
[24] M. Ulbricht, G. Belfort, Surface modification of ultrafiltration membranes by low temperature plasma II. Graft polymerization onto polyacrylonitrile and polysulfone, J. Membr. Sci., 111 (1996) 193–215.
[25] J.-E. An, G.W. Jeon, Y.G. Jeong, Preparation and properties of polypropylene nanocomposites reinforced with exfoliated graphene, Fibers Polym., 13 (2012) 507–514.
[26] N. Pasquini, Polypropylene Handbook, Middle East, (2005) 254–256.
[27] J. Pieracci, J.V. Crivello, G. Belfort, Increasing membrane permeability of UV-modified poly (ether sulfone) ultrafiltration membranes, J. Membr. Sci., 202 (2002) 1–16.
[28] I. Kim, J. Choi, T. Tak, Sulfonated polyethersulfone by heterogeneous method and its membrane performances, J. Appl. Polym. Sci., 74 (1999) 2046–2055.
[29] H.-Y. Yu, M.-X. Hu, Z.-K. Xu, J.-L. Wang, S.-Y. Wang, Surface modification of polypropylene microporous membranes to improve their antifouling property in MBR: NH_3 plasma treatment, Sep. Purif. Technol., 45 (2005) 8–15.
[30] G. Wu, S. Gan, L. Cui, Y. Xu, Preparation and characterization of PES/TiO_2 composite membranes, Appl. Surf. Sci., 254 (2008) 7080–7086.

[31] L. Liu, C. Zhao, F. Yang, TiO_2 and polyvinyl alcohol (PVA) coated polyester filter in bioreactor for wastewater treatment, Water Res., 46 (2012) 1969–1978.
[32] M. Homayoonfal, M.R. Mehrnia, S. Rahmani, Y.M. Mojtahedi, Fabrication of alumina/polysulfone nanocomposite membranes with biofouling mitigation approach in membrane bioreactors, J. Ind. Eng. Chem., 22 (2015) 357–367.
[33] T.-H. Bae, T.-M. Tak, Effect of TiO_2 nanoparticles on fouling mitigation of ultrafiltration membranes for activated sludge filtration, J. Membr. Sci., 249 (2005) 1–8.
[34] G. Gesan-Guiziou, R. Wakeman, G. Daufin, Stability of latex crossflow filtration: cake properties and critical conditions of deposition, Chem. Eng. J., 85 (2002) 27–34.
[35] M. Ahsani, R. Yegani, Study on the fouling behavior of silica nanocomposite modified polypropylene membrane in purification of collagen protein, Chem. Eng. Res. Des., 102 (2015) 261–273.
[36] B. Luo, Z. Li, J. Zhang, X. Wang, Formation of anisotropic microporous isotactic polypropylene (iPP) membrane via thermally induced phase separation, Desalination, 233 (2008) 19–31.
[37] M. Mulder, Basic Principles of Membrane Technology, Springer Science & Business Media, Netherland (1996).
[38] J. Hermia, Constant pressure blocking filtration law application to powder-law non-Newtonian fluid, Trans. Inst. Chem. Eng., 60 (1982) 183–187.
[39] C. Rai, P. Rai, G. Majumdar, S. De, S. DasGupta, Mechanism of permeate flux decline during microfiltration of watermelon (*Citrullus lanatus*) juice, Food Bioprocess Technol., 3 (2010) 545–553.
[40] G. Bolton, D. LaCasse, R. Kuriyel, Combined models of membrane fouling: development and application to microfiltration and ultrafiltration of biological fluids, J. Membr. Sci., 277 (2006) 75–84.
[41] W.R. Bowen, J.I. Calvo, A. Hernández, Steps of membrane blocking in flux decline during protein microfiltration, J. Membr. Sci., 101 (1995) 153–165.
[42] H.H. Fang, X. Shi, Pore fouling of microfiltration membranes by activated sludge, J. Membr. Sci., 264 (2005) 161–166.
[43] Y. Jafarzadeh, R. Yegani, Analysis of fouling mechanisms in TiO_2 embedded high density polyethylene membranes for collagen separation, Chem. Eng. Res. Des., 93 (2015) 684–695.
[44] F. Shi, J. Ma, P. Wang, Y. Ma, Effect of quenching temperatures on the morphological and crystalline properties of PVDF and PVDF–TiO_2 hybrid membranes, J. Taiwan Inst. Chem. Eng., 43 (2012) 980–988.
[45] V. Vatanpour, S.S. Madaeni, A.R. Khataee, E. Salehi, S. Zinadini, H.A. Monfared, TiO_2 embedded mixed matrix PES nanocomposite membranes: influence of different sizes and types of nanoparticles on antifouling and performance, Desalination, 292 (2012) 19–29.
[46] F.S. Dehkordi, M. Pakizeh, M. Namvar-Mahboub, Properties and ultrafiltration efficiency of cellulose acetate/organically modified Mt (CA/OMMt) nanocomposite membrane for humic acid removal, Appl. Clay Sci., 105 (2015) 178–185.
[47] P. Le-Clech, V. Chen, T.A. Fane, Fouling in membrane bioreactors used in wastewater treatment, J. Membr. Sci., 284 (2006) 17–53.
[48] V. Chen, K. Kim, A. Fane, Effect of membrane morphology and operation on protein deposition in ultrafiltration membranes, Biotechnol. Bioeng., 47 (1995) 174–180.
[49] K. Kim, V. Chen, A. Fane, Some factors determining protein aggregation during ultrafiltration, Biotechnol. Bioeng., 42 (1993) 260–265.